

The effect of the accuracies of flexure hinge equations on the output compliances of planar micro-motion stages

Yuen Kuan Yong *, Tien-Fu Lu

School of Mechanical Engineering, The University of Adelaide, SA 5005, Australia

Received 23 May 2006; received in revised form 20 February 2007; accepted 22 March 2007

Available online 28 June 2007

Abstract

This paper presents the effect of the accuracies of flexure hinge compliance equations (the accuracies vary with a geometrical ratio, t/R of a hinge) on the output compliances of RRR and 3-RRR micro-motion stages. Closed-form output compliance models of the stages are derived (with flexure hinge compliances as one of the variables) to investigate the aforementioned effect. The output compliances, calculated using various flexure hinge equations, are compared to that of the finite element analysis (FEA) and the results are discussed.

Crown Copyright © 2007 Published by Elsevier Ltd. All rights reserved.

Keywords: Micro-motion stage; Output compliance; Flexure hinge equation

1. Introduction

Compliant micro-motion stages have emerged as an important technological advancement due to its growing applications in the field of micro-machining, scanning electron microscopy, assembly of micro-systems, the alignments of fibre-optic and laser, micro-lithography and biological cell manipulation. Compliant stages, which consist of flexure hinges, are capable of providing smooth motions through structural deformations.

Kinematic, static and dynamic models are needed to analyse and to synthesise the behaviour of a particular compliant stage design. In order to improve the accuracy of these models, the modelling of flexure hinge deformations and compliances (inverse of stiffness) are required to be accurate. Various flexure hinge compliance equations were derived to predict the deformation and stiffness of a flexure hinge. Methods such as the inverse conformal mapping [1], finite element analysis [2–4], the Castigliano's second theorem [5,6] or the integration of linear differential equations of beams [5,7] have been used to derive an accurate flexure hinge model. However, depending on the geometrical ratio of flexure hinges, t/R (see Fig. 1 for hinge geometries), some of these methods are more accurate than others. To support this statement, comparisons of flexure hinge compliances were carried out as shown in Figs. 2–4. The compliance of a flexure hinge modelled using FEA (ANSYS) was

* Corresponding author. Tel.: +61 883036385; fax: +61 883034367.

E-mail addresses: yuen.yong@mecheng.adelaide.edu.au, Yuenkuan.Yong@newcastle.edu.au (Y.K. Yong).

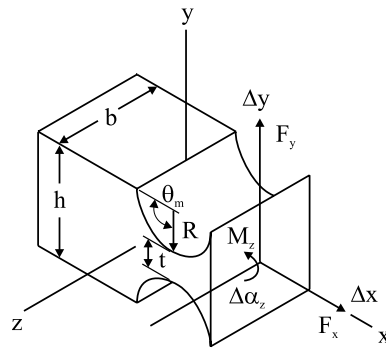


Fig. 1. Schematic of flexure hinge with dimensions, local coordinate, applied forces/moments and displacements.

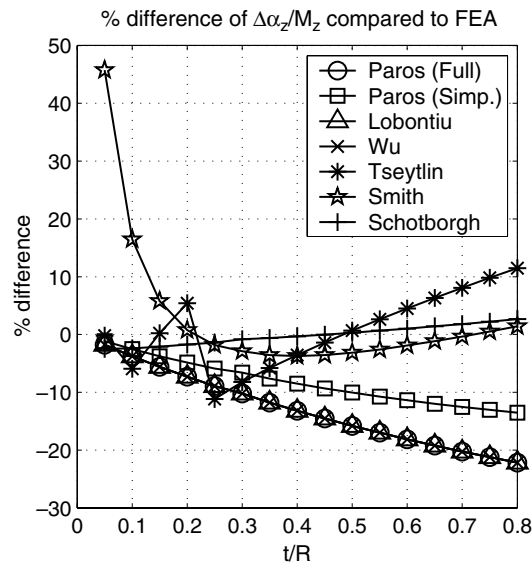


Fig. 2. Comparison of flexure hinge rotational compliances ($\Delta\alpha_z/M_z$) to FEA results.

used as a benchmark for the comparisons. From Figs. 2–4, it can be seen that flexure hinge compliances determined using any single particular method will not be accurate for a large range of t/R ratios.

The effect of the accuracies of flexure hinge compliance equations on the output compliances of micro-motion stages has not been studied. As a result, simple closed-form equations (with flexure hinge compliances as one of the variables) are derived in this paper to determine the output compliances of a RRR (revolute–revolute–revolute) and a 3-RRR stage in order to study the effect mentioned above. The RRR compliant structure consists of three flexure hinges, and the 3-RRR structure consists of three RRR chains connected together in parallel as shown in Fig. 5. The parallel configuration of the 3-RRR structure is advantageous over a serial configuration structure. Parallel structures provide high mechanical stiffness, high motion accuracy and high resonant frequency, which make parallel structures suitable for micro-positioning applications.

Literatures were carried out to study the existing methods used to model compliant micro-motion stages. The pseudo-rigid-body-model (PRBM) method is commonly used to predict the displacements of compliant mechanisms with flexure hinges. The PRBM commonly models a flexure hinge as a revolute joint (1-DOF) with an attached torsional spring. The PRBM method is effective and it simplifies the model of compliant mechanisms; however the PRBM results showed some inaccuracies when the axial and transverse deformations¹ were

¹ Axial deformation refers to the deformation of a flexure hinge in the x -axis (see Fig. 1 for axis labels). Transverse deformation refers to the deformation of a flexure hinge in the y -axis.

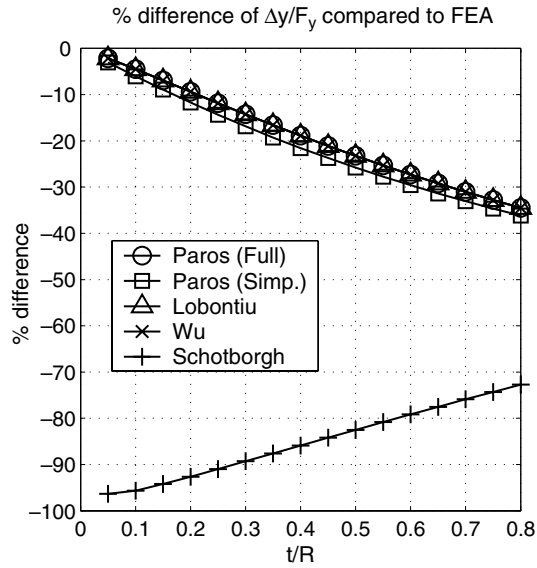


Fig. 3. Comparison of flexure hinge transverse compliances ($\Delta y/F_y$) to FEA results.

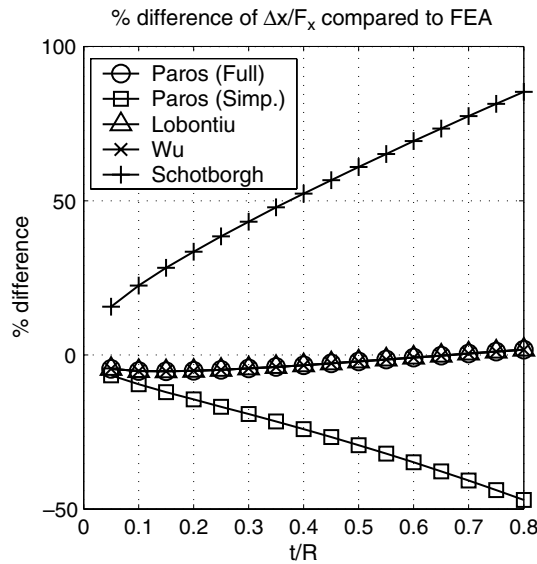


Fig. 4. Comparison of flexure hinge axial compliances ($\Delta x/F_x$) to FEA results.

not incorporated into the model [2,8–11]. Pham et al. [12] derived a kinematic model of a flexure parallel mechanism using an extended PRBM method, named the PRB-D method. The PRB-D method models flexure hinges to have all 6-DOF. They applied the PRBM and the PRB-D kinematic results to control the mechanism and the PRB-D results produced only 1/3 the error of the PRBM results. The output compliance modeling of the mechanism is not derived. The effect of the accuracies of flexure hinge equations on the output compliances is not presented.

Jouaneh and Yang [13] developed a mathematical model to predict the displacement and stiffness of a vertical motion compliant stage. Axial and transverse deformations of hinge are considered in the analytical model. Lobontiu and Garcia [14] formulated an analytical method for displacement and stiffness calculations of planar compliant mechanisms with flexure hinges. The closed-form formulations were based on strain

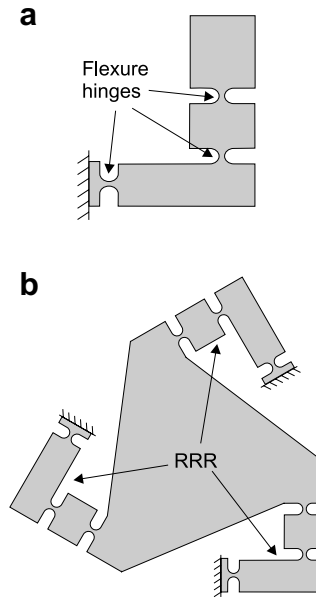


Fig. 5. Compliant micro-motion stages. (a) RRR and (b) 3-RRR.

energy and Castigliano's displacement theorem. However, the methods developed by Jouaneh & Yang and Lobontiu & Garcia were only applied to 1-DOF compliant mechanisms and it is not clear if these methods would be applicable to multi-DOF compliant mechanisms. The influence of the flexure hinge modelling accuracies on the output compliances of the stages are not discussed.

Gao et al. [15] derived a static model for a 2-DOF compliant stage. Axial deformations of flexure hinges were considered in these models. Paros and Weisbord's simplified equations [7] were used to calculate both the rotational and axial compliances of flexure hinges. Hsiao and Lin [5] derived a static model for a RRR compliant structure with three flexure hinges. They derived the relationship between external applied loads and deflections at the loading point. This method was not used to model a 3-RRR compliant mechanism and it was not clear if this method would be applicable to those type of mechanisms. The effect of the accuracies of flexure hinge equations on the output compliances is not presented.

Pham and Chen [16] derived analytical models to estimate the output stiffness of a 3-DOF translational flexure parallel mechanism (FPM). The FPM consists of three double compound linear structures, and three 3-RRR compliant mechanisms. They modelled flexure hinges to have all 6-DOF. Ryu et al. [17] developed a $XY\theta$ compliant stage which was driven by three piezoelectric actuators. The topology of this stage is similar to a 3-RRR mechanism except it consists of a double compound lever at each of the three input linkages. They formulated a mathematical model to describe the relationship between input and output displacements of the stage, by considering compliances of flexure hinges in all six axes. However, the modeling methods of Pham & Chen and Ryu et al. involve an intensive number of coordinate transformations and the methods may be complicated. The influence of the flexure hinge modelling accuracies on the output compliances of the stages are not presented.

Although there are various analytical models developed to calculate displacements and compliances of micro-motion stages, only a few research groups derived output compliance models for RRR and 3-RRR micro-motion stages. Accuracies of these developed models are partly influenced by the accuracies of the flexure hinge equations used in the models; however this issue has not been investigated. Flexure hinge compliance equations were previously derived using methods such as the Castigliano's second theorem [5,6], finite element analysis [2–4] and the integration of linear differential equations of beams [5,7]. As shown in Figs. 2–4, some of these flexure hinge compliance equations however provide better accuracies than the others depending on the t/R ratio of a hinge. There is a lack of literatures up to this date reporting the effect of the accuracies of flexure hinge equations on the output compliances of micro-motion stages.

This paper presents the effect of the accuracies of flexure hinge equations on the output compliances of RRR and 3-RRR micro-motion stages. Simple closed-form equations are derived to determine the output compliances of the stages. The closed-form output compliance equations are expressed in terms of flexure hinge compliances, material properties and geometrical parameters. Since flexure hinge compliances are one of the variables in the equations, previously derived flexure hinge compliances equations [3,6,7,18], which have different modelling accuracies depending on different t/R ratios of flexure hinges (see Figs. 2–4) are used to calculate the output compliances of the micro-motion stages. The results of the output compliances are compared to the FEA results to verify their accuracies.

2. The derivation of the output compliance matrix of the RRR compliant micro-motion stage

A RRR compliant stage is shown in Fig. 6 together with its dimensions, displacements, local coordinates of flexure hinges and the applied forces/moments. The compliances at point o' contributed by each flexure hinge in the structure are firstly calculated. The overall compliances of the RRR compliant stage at point o' are then obtained by summing all compliances (in the corresponding directions) contributed by each individual flexure

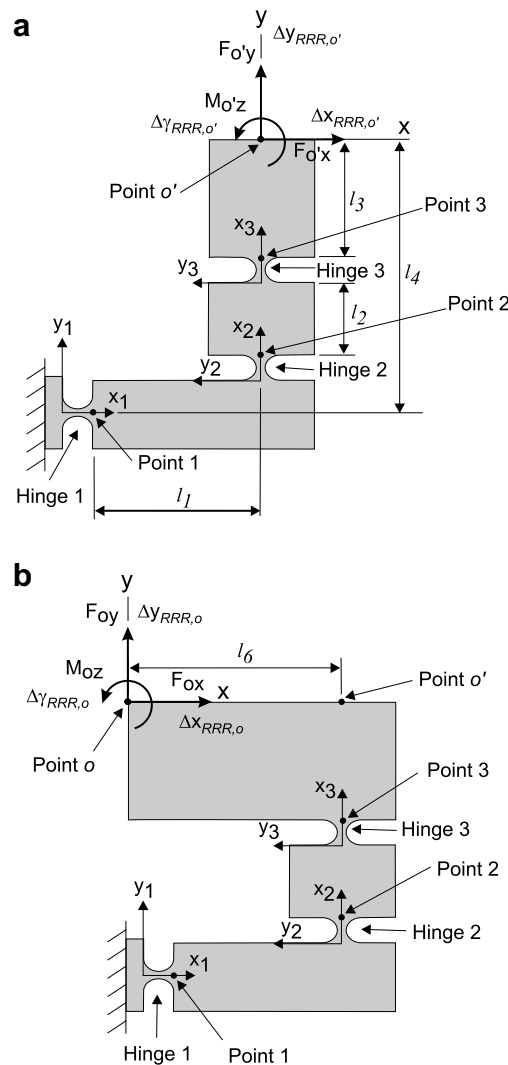


Fig. 6. RRR compliant mechanism with dimensions, local coordinates of flexure hinges, hinge and point labels. (a) Applied forces/moments at output point o' . (b) Applied forces/moments at output point o .

hinges. $\Delta\alpha$, Δy and Δx are the rotational motions about the z -axis and the translational motions in the y - and x -axis, respectively. Similarly, $C\Delta\alpha$, $C\Delta y$ and $C\Delta x$ are the rotational and translational compliances along the corresponding axes. The subscripts “ $o'i, F_{o'x}$ ”, “ $o'i, F_{o'y}$ ” and “ $o'i, M_{o'z}$ ” indicate the displacements/compliances at point o' due to compliances of hinge i ($i = 1, 2, 3$) when output forces/moments, $F_{o'x}$, $F_{o'y}$ and $M_{o'z}$ are applied. $[\Delta\alpha_z/M_z]_i$, $[\Delta y/F_y]_i$ and $[\Delta x/F_x]_i$ are compliances of Hinge i which can be calculated using previously derived equations [1,3,4,6,7,18,19]. The effect of the accuracies of these flexure hinge equations on the output compliance results of the micro-motion stages are studied.

Noted that all flexure hinges are modelled to have 3-DOF (rotational compliance about the z -axis, axial and transverse compliances in the x - and the y -axis). Flexure hinges are modelled as having 3-DOF instead of 6-DOF due to the fact that both the RRR and 3-RRR compliant stages studied in this paper are planar. Out-of-plane compliances are very small for thick hinges (b is large), and therefore the out-of-plane compliances are neglected in order to simplify the modelling equations.

2.1. Output compliances due to Hinge 1

2.1.1. Rotational compliances about the z -direction of a RRR compliant stage

When output force, $F_{o'x}$ is applied,

$$\Delta\alpha_{o'1, F_{o'x}} = - \left[\frac{\Delta\alpha_z}{M_z} \right]_1 (F_{o'x} \cdot l_4) \tag{1}$$

$$C\Delta\alpha_{o'1, F_{o'x}} = \frac{\Delta\alpha_{o'1, F_{o'x}}}{F_{o'x}} = - \left[\frac{\Delta\alpha_z}{M_z} \right]_1 \cdot l_4 \tag{2}$$

When output force, $F_{o'y}$ is applied,

$$\Delta\alpha_{o'1, F_{o'y}} = \left[\frac{\Delta\alpha_z}{M_z} \right]_1 F_{o'y} (l_1 + R_1) \tag{3}$$

$$C\Delta\alpha_{o'1, F_{o'y}} = \left[\frac{\Delta\alpha_z}{M_z} \right]_1 (l_1 + R_1) \tag{4}$$

When output moment, $M_{o'z}$ is applied,

$$C\Delta\alpha_{o'1, M_{o'z}} = \left[\frac{\Delta\alpha_z}{M_z} \right]_1 \tag{5}$$

2.1.2. Translational compliances in the y -direction of a RRR compliant stage

When output force, $F_{o'x}$ is applied, the output translational compliance in the y -direction is caused by the rotational displacement of the hinge (see Fig. 7),

$$\Delta y_{o'1, F_{o'x}} = - \left[\frac{\Delta\alpha_z}{M_z} \right]_1 (F_{o'x} \cdot l_4) \cdot (l_1 + R_1) \tag{6}$$

$$C\Delta y_{o'1, F_{o'x}} = - \left[\frac{\Delta\alpha_z}{M_z} \right]_1 l_4 \cdot (l_1 + R_1) \tag{7}$$

When output force, $F_{o'y}$ is applied, the output compliance in the y -direction at point 1 (see Fig. 8) is,

$$\Delta y_{1, F_{o'y}} = \left\{ \left[\frac{\Delta\alpha_z}{M_z} \right]_1 \cdot R_1 \cdot F_{o'y} l_1 + \left[\frac{\Delta y}{F_y} \right]_1 \cdot F_{o'y} \right\} \tag{8}$$

$$C\Delta y_{1, F_{o'y}} = \left\{ \left[\frac{\Delta\alpha_z}{M_z} \right]_1 \cdot R_1 l_1 + \left[\frac{\Delta y}{F_y} \right]_1 \right\} \tag{9}$$

The first term of $C\Delta y_{1, F_{o'y}}$ represents the compliance in the y -direction of point 1 caused by moment $F_{o'y} l_1$ and the second term represents the compliance in the y -direction caused by force $F_{o'y}$.

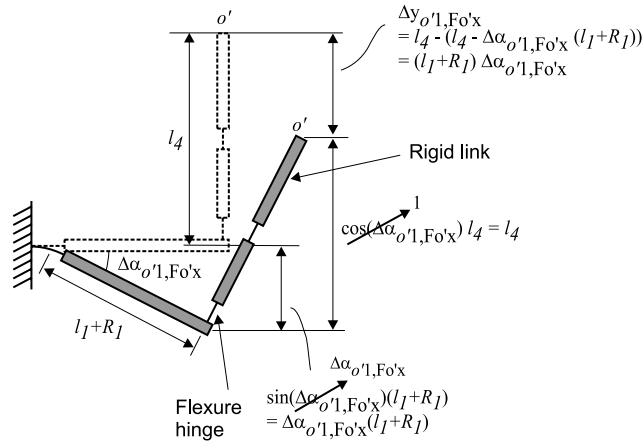


Fig. 7. Calculation of $\Delta y_{o'1, F_{o'x}}$. Dashed lines represent initial position of the RRR structure. Flexure hinge is drawn as a solid line and rigid link is drawn as a block.

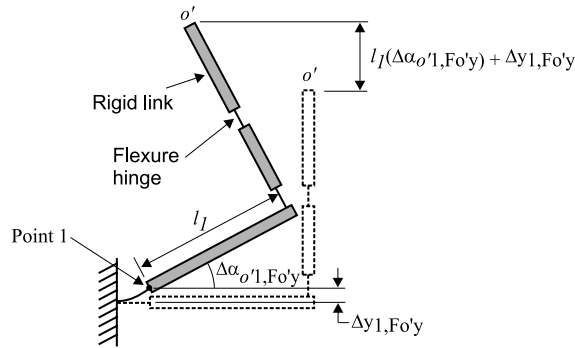


Fig. 8. Calculation of $\Delta y_{o'1, F_{o'y}}$. Dashed lines represent initial position of the RRR structure. Flexure hinge is drawn as a solid line and rigid link is drawn as a block.

Thus, from Eqs. (4) and (9), $C\Delta y_{o'1, F_{o'y}}$ can be calculated (see Fig. 8),

$$\begin{aligned}
 C\Delta y_{o'1, F_{o'y}} &= \frac{\Delta\alpha_{o'1, F_{o'y}} \cdot l_1 + \Delta y_{1, F_{o'y}}}{F_{o'y}} = C\Delta\alpha_{o'1, F_{o'y}} \cdot l_1 + C\Delta y_{1, F_{o'y}} \\
 &= \left[\frac{\Delta\alpha_z}{M_z} \right]_1 \{R_1 l_1 + l_1(l_1 + R_1)\} + \left[\frac{\Delta y}{F_y} \right]_1
 \end{aligned} \tag{10}$$

When output moment, $M_{o'z}$ is applied,

$$\Delta y_{o'1, M_{o'z}} = \left[\frac{\Delta\alpha_z}{M_z} \right]_1 M_{o'z} \cdot (l_1 + R_1) \tag{11}$$

$$C\Delta y_{o'1, M_{o'z}} = \left[\frac{\Delta\alpha_z}{M_z} \right]_1 (l_1 + R_1) \tag{12}$$

2.1.3. Translational compliances in the x-direction of a RRR compliant stage

When output force, $F_{o'x}$ is applied,

$$\Delta x_{o'1, F_{o'x}} = \left[\frac{\Delta x}{F_x} \right]_1 F_{o'x} - \Delta\alpha_{o'1, F_{o'x}} \cdot l_4 \tag{13}$$

where the first term of $\Delta x_{o'1,F_{o'x}}$ represents the x -displacement of point o' caused by the compliance in the x -direction of Hinge 1. The second term represents the x -displacement caused by the amplification of links (with distance of l_4).

From Eq. (13),

$$C\Delta x_{o'1,F_{o'x}} = \frac{\Delta x_{o'1,F_{o'x}}}{F_{o'x}} = \left[\frac{\Delta x}{F_x} \right]_1 - C\Delta\alpha_{o'1,F_{o'x}} \cdot l_4 = \left[\frac{\Delta x}{F_x} \right]_1 + \left[\frac{\Delta\alpha_z}{M_z} \right]_1 l_4^2 \tag{14}$$

where $C\Delta\alpha_{o'1,F_{o'x}}$ is obtained from Eq. (2).

When output force, $F_{o'y}$ is applied,

$$\Delta x_{o'1,F_{o'y}} = -\Delta\alpha_{o'1,F_{o'y}} \cdot l_4 \tag{15}$$

$$C\Delta x_{o'1,F_{o'y}} = -C\Delta\alpha_{o'1,F_{o'y}} \cdot l_4 = -\left[\frac{\Delta\alpha_z}{M_z} \right]_1 (l_1 + R_1)l_4 \tag{16}$$

where $C\Delta\alpha_{o'1,F_{o'y}}$ is obtained from Eq. (4).

When output moment, $M_{o'z}$ is applied,

$$C\Delta x_{o'1,M_{o'z}} = -\left[\frac{\Delta\alpha_z}{M_z} \right]_1 l_4 \tag{17}$$

where $C\Delta\alpha_{o'1,M_{o'z}}$ is obtained from Eq. (5).

Thus, the output compliance matrix of RRR mechanism at point o' due to compliances of Hinge 1 is,

$$C_1 = \begin{bmatrix} C\Delta x_{o'1,F_{o'x}} & C\Delta x_{o'1,F_{o'y}} & C\Delta x_{o'1,M_{o'z}} \\ C\Delta y_{o'1,F_{o'x}} & C\Delta y_{o'1,F_{o'y}} & C\Delta y_{o'1,M_{o'z}} \\ C\Delta\alpha_{o'1,F_{o'x}} & C\Delta\alpha_{o'1,F_{o'y}} & C\Delta\alpha_{o'1,M_{o'z}} \end{bmatrix} \tag{18}$$

Displacements of RRR mechanism at point o' due to compliances of Hinge 1 when output forces/moments are applied are,

$$[\Delta X_{o'1} \quad \Delta Y_{o'1} \quad \Delta\gamma_{o'1}]^T = C_1 \times F_{o'} \tag{19}$$

where $F_{o'} = [F_{o'x} \quad F_{o'y} \quad M_{o'z}]^T$.

2.2. Output compliances due to Hinge 2

The compliances of RRR mechanism due to Hinge 2 are calculated in the local coordinate (x_2, y_2) of Hinge 2 (see Fig. 6). This compliance matrix will be rotated by 90° when the summation of all the three compliance matrices (C_1, C_2, C_3) of flexure hinges are conducted to obtain the overall output compliance matrix of the RRR mechanism. Similar procedures are carried out as presented in Section 2.1 and the following compliances are obtained.

2.2.1. Rotational compliances about the z-direction of a RRR compliant stage

When output force, $F_{o'x}$ is applied,

$$C\Delta\alpha_{o'2,F_{o'x}} = -\left[\frac{\Delta\alpha_z}{M_z} \right]_2 (l_2 + l_3 + R_2 + 2R_3) \tag{20}$$

When output force, $F_{o'y}$ is applied,

$$C\Delta\alpha_{o'2,F_{o'y}} = 0 \tag{21}$$

When output force, $M_{o'z}$ is applied,

$$C\Delta\alpha_{o'2,M_{o'z}} = \left[\frac{\Delta\alpha_z}{M_z} \right]_2 \tag{22}$$

2.2.2. Translational compliances in the y-direction of a RRR compliant stage

When output force, $F_{o'x}$ is applied, the compliance in the y-direction (local coordinate) at point 2 is,

$$C\Delta y_{2,F_{o'x}} = - \left\{ \left[\frac{\Delta\alpha_z}{M_z} \right]_2 \cdot R_2(l_2 + l_3 + 2R_3) + \left[\frac{\Delta y}{F_y} \right]_2 \right\} \quad (23)$$

The procedure of calculating $C\Delta y_{o'2,F_{o'x}}$ is similar to $C\Delta y_{o'1,F_{o'x}}$. The first term of $C\Delta y_{2,F_{o'x}}$ represents the compliance in the y-direction of point 2 caused by moment, $F_{o'x}(l_2 + l_3 + 2R_3)$ and the second term represents the compliance in the y-direction caused by force, $F_{o'x}$.

Thus,

$$\begin{aligned} C\Delta y_{o'2,F_{o'x}} &= \frac{\Delta\alpha_{o'2,F_{o'x}} \cdot (l_2 + l_3 + 2R_3) + \Delta y_{2,F_{o'x}}}{F_{o'x}} = C\Delta\alpha_{o'2,F_{o'x}} \cdot (l_2 + l_3 + 2R_3) + C\Delta y_{2,F_{o'x}} \\ &= - \left[\frac{\Delta\alpha_z}{M_z} \right]_2 (l_2 + l_3 + 2R_3)(l_2 + l_3 + 2R_2 + 2R_3) - \left[\frac{\Delta y}{F_y} \right]_2 \end{aligned} \quad (24)$$

where $C\Delta\alpha_{o'2,F_{o'x}}$ is obtained from Eq. (20) and $C\Delta y_{2,F_{o'x}}$ is obtained from Eq. (23).

When output force, $F_{o'y}$ is applied,

$$C\Delta y_{o'2,F_{o'y}} = 0 \quad (25)$$

When output force, $M_{o'z}$ is applied,

$$C\Delta y_{o'2,M_{o'z}} = \left[\frac{\Delta\alpha_z}{M_z} \right]_2 (l_2 + l_3 + R_2 + 2R_3) \quad (26)$$

2.2.3. Translational compliances in the x-direction of a RRR compliant stage

When output force, $F_{o'x}$ is applied,

$$C\Delta x_{o'2,F_{o'x}} = 0 \quad (27)$$

When output force, $F_{o'y}$ is applied,

$$C\Delta x_{o'2,F_{o'y}} = \left[\frac{\Delta x}{F_x} \right]_2 \quad (28)$$

When output force, $M_{o'z}$ is applied,

$$C\Delta\alpha_{o'2,M_{o'z}} = 0 \quad (29)$$

Thus, the output compliance matrix of RRR mechanism at point o' due to compliances of Hinge 2 is,

$$C_2 = \begin{bmatrix} C\Delta x_{o'2,F_{o'x}} & C\Delta x_{o'2,F_{o'y}} & C\Delta x_{o'2,M_{o'z}} \\ C\Delta y_{o'2,F_{o'x}} & C\Delta y_{o'2,F_{o'y}} & C\Delta y_{o'2,M_{o'z}} \\ C\Delta\alpha_{o'2,F_{o'x}} & C\Delta\alpha_{o'2,F_{o'y}} & C\Delta\alpha_{o'2,M_{o'z}} \end{bmatrix} \quad (30)$$

Displacements of RRR mechanism at o' due to compliances of Hinge 2, when output forces/moments are applied are,

$$[\Delta X_{o'2} \quad \Delta Y_{o'2} \quad \Delta\gamma_{o'2}]^T = C_2 \times F_{o'} \quad (31)$$

2.3. Output compliances due to Hinge 3

Similar to Section 2.2, compliances of RRR mechanism due to Hinge 3 are calculated in the local coordinate (x_3, y_3) of Hinge 3. This compliance matrix will be rotated by 90° when the summation of all the three compliance matrices (C_1, C_2, C_3) of flexure hinges are conducted to obtain the overall output compliance matrix of the RRR stage.

2.3.1. Rotational compliances about the z-direction of a RRR compliant stage

When output force, $F_{o'x}$ is applied,

$$C\Delta\alpha_{o'3,F_{o'x}} = - \left[\frac{\Delta\alpha_z}{M_z} \right]_3 \cdot (l_3 + R_3) \quad (32)$$

When output force, $F_{o'y}$ is applied,

$$C\Delta\alpha_{o'3,F_{o'y}} = 0 \quad (33)$$

When output force, $M_{o'z}$ is applied,

$$C\Delta\alpha_{o'3,M_{o'z}} = \left[\frac{\Delta\alpha_z}{M_z} \right]_3 \quad (34)$$

2.3.2. Translational compliances in the y-direction of a RRR compliant stage

When output force, $F_{o'x}$ is applied, the compliance in the y-direction (local coordinate) at point 3 is,

$$C\Delta y_{3,F_{o'x}} = - \left\{ \left[\frac{\Delta\alpha_z}{M_z} \right]_3 \cdot R_3 \cdot l_3 + \left[\frac{\Delta y}{F_y} \right]_3 \right\} \quad (35)$$

Thus, from Eqs. (32) and (35),

$$C\Delta y_{o'3,F_{o'x}} = C\Delta\alpha_{o'3,F_{o'x}} \cdot l_3 + C\Delta y_{3,F_{o'x}} = - \left[\frac{\Delta\alpha_z}{M_z} \right]_3 (l_3 + 2R_3)l_3 - \left[\frac{\Delta y}{F_y} \right]_3 \quad (36)$$

When output force, $F_{o'y}$ is applied,

$$C\Delta y_{o'3,F_{o'y}} = 0 \quad (37)$$

When output force, $M_{o'z}$ is applied,

$$C\Delta y_{o'3,M_{o'z}} = \left[\frac{\Delta\alpha_z}{M_z} \right]_3 (l_3 + R_3) \quad (38)$$

2.3.3. Translational compliances in the x-direction of a RRR compliant stage

When output force, $F_{o'x}$ is applied,

$$C\Delta x_{o'3,F_{o'x}} = 0 \quad (39)$$

When output force, $F_{o'y}$ is applied,

$$C\Delta x_{o'3,F_{o'y}} = \left[\frac{\Delta x}{F_x} \right]_3 \quad (40)$$

When output moment, $M_{o'z}$ is applied,

$$C\Delta x_{o'3,M_{o'z}} = 0 \quad (41)$$

Thus, the output compliance matrix of RRR mechanism at point o' due to compliances of Hinge 3 is,

$$C_3 = \begin{bmatrix} C\Delta x_{o'3,F_{o'x}} & C\Delta x_{o'3,F_{o'y}} & C\Delta x_{o'3,M_{o'z}} \\ C\Delta y_{o'3,F_{o'x}} & C\Delta y_{o'3,F_{o'y}} & C\Delta y_{o'3,M_{o'z}} \\ C\Delta\alpha_{o'3,F_{o'x}} & C\Delta\alpha_{o'3,F_{o'y}} & C\Delta\alpha_{o'3,M_{o'z}} \end{bmatrix} \quad (42)$$

Displacements of RRR mechanism at point o' due to compliances of Hinge 3 when output forces/moments are applied,

$$[\Delta X_{o'3} \quad \Delta Y_{o'3} \quad \Delta \gamma_{o'3}]^T = C_3 \times F_{o'} \quad (43)$$

2.4. Output compliances of RRR compliant mechanism

The output compliance matrix of the RRR mechanism at point o' is equal to the sum of all the three compliance matrices, C_1 , C_2 and C_3 . C_2 and C_3 are derived in their local coordinates (x_2-y_2 and x_3-y_3) which are orientated 90° from x_1-y_1 . Therefore, C_2 and C_3 matrices are rotated by 90° before the summation.

$$C_{RRR,o'} = C_1 + T_{\pi/2} \times C_2 + T_{\pi/2} \times C_3 \tag{44}$$

where,

$$T_{\pi/2} = \begin{bmatrix} \cos(\pi/2) & -\sin(\pi/2) & 0 \\ \sin(\pi/2) & \cos(\pi/2) & 0 \\ 0 & 0 & 1 \end{bmatrix} \tag{45}$$

The output displacements at point o' of the RRR mechanism is,

$$[\Delta x_{RRR} \quad \Delta y_{RRR} \quad \Delta \gamma_{RRR}]_{o'}^T = C_{RRR,o'} \times F_{o'} \tag{46}$$

When output forces are applied at point o instead of point o' (see Fig. 6b) and the displacements at this point are desired, matrix T_f can be used to transfer the output forces from point o to point o' . Once $C_{RRR,o'}$ is determined using Eq. (44), a compliance matrix at point o can be calculated by transforming $C_{RRR,o'}$ to point o using a matrix, T_d . Intuitively, we know that $\Delta x_{RRR,o} = \Delta x_{RRR,o'}$ and $\Delta \gamma_{RRR,o} = \Delta \gamma_{RRR,o'}$. However, $\Delta y_{RRR,o} \neq \Delta y_{RRR,o'}$ due to rotational motions ($\Delta \gamma_{RRR,o}$) and the amplification of lever arm, l_6 . Displacement, $\Delta y_{RRR,o}$ of the RRR stage is illustrated in Fig. 9.

The force transformation matrix is,

$$T_f = \begin{bmatrix} 1 & 0 & 0 \\ 0 & 1 & 0 \\ 0 & -l_6 & 1 \end{bmatrix} \tag{47}$$

The displacement transformation matrix is,

$$T_d = \begin{bmatrix} 1 & 0 & 0 \\ 0 & 1 & -l_6 \\ 0 & 0 & 1 \end{bmatrix} \tag{48}$$

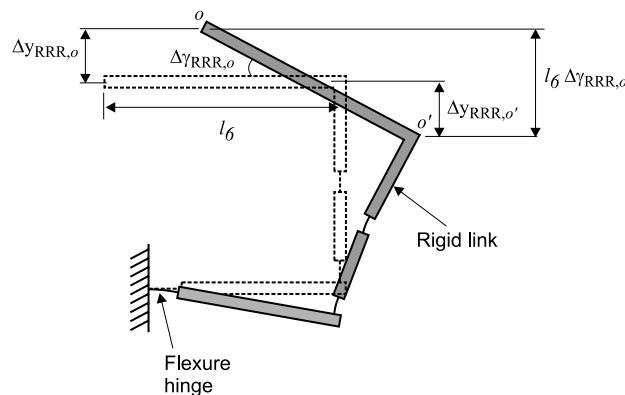


Fig. 9. Calculation of compliances at point o . Dashed lines represent initial position of the RRR structure. Flexure hinge is drawn as a solid line and rigid link is drawn as a block.

Therefore, the output displacements at o of the RRR mechanism is,

$$\begin{bmatrix} \Delta x_{RRR} \\ \Delta y_{RRR} \\ \Delta \gamma_{RRR} \end{bmatrix}_o = T_d \times C_{RRR,o'} \times (T_f \times F_o) \tag{49}$$

Thus, the output compliances at point o is,

$$C_{RRR,o} = T_d \times C_{RRR,o'} \times T_f \tag{50}$$

where $F_o = [F_{ox} \ F_{oy} \ M_{oz}]^T$.

3. Output compliance matrix of 3-RRR compliant micro-motion stage

The 3-RRR compliant micro-motion stage is generated by arranging the three RRR compliant stages 120° apart (see Fig. 10a). A spring model of the 3-RRR compliant stage is developed as shown in Fig. 10b. Each of the box represents the compliance matrix of each RRR link, C_{RRR1} , C_{RRR2} and C_{RRR3} . The compliance matrices of RRR link 2 and 3 are rotated by 120° and -120° , respectively.

Displacements ($D_{RRR2,o}$ and $D_{RRR3,o}$) at output point, o due to compliances of RRR link 2 and 3, respectively are,

$$D_{RRR2,o} = T_{2\pi/3} \times C_{RRR,o} \times T_{2\pi/3}^T \times F_o \tag{51}$$

$$D_{RRR3,o} = T_{-2\pi/3} \times C_{RRR,o} \times T_{-2\pi/3}^T \times F_o \tag{52}$$

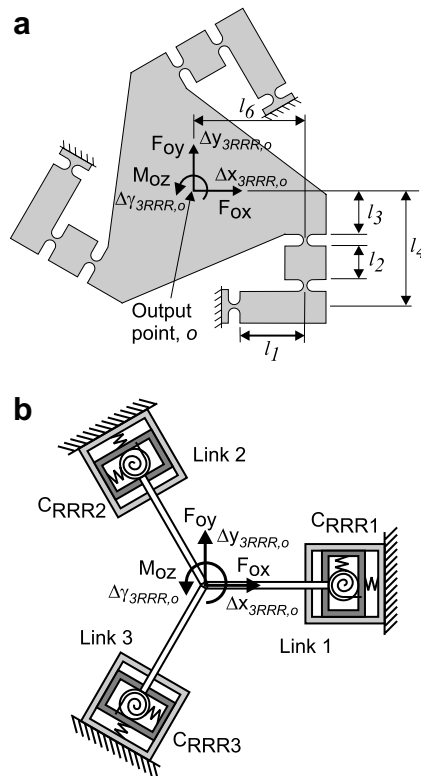


Fig. 10. (a) 3-RRR compliant micro-motion stage. (b) Spring model of 3-RRR compliant micro-motion stage.

where,

$$T_{2\pi/3} = \begin{bmatrix} \cos(2\pi/3) & -\sin(2\pi/3) & 0 \\ \sin(2\pi/3) & \cos(2\pi/3) & 0 \\ 0 & 0 & 1 \end{bmatrix} \tag{53}$$

$$T_{-2\pi/3} = \begin{bmatrix} \cos(-2\pi/3) & -\sin(-2\pi/3) & 0 \\ \sin(-2\pi/3) & \cos(-2\pi/3) & 0 \\ 0 & 0 & 1 \end{bmatrix} \tag{54}$$

$T_{2\pi/3}^T$ and $T_{-2\pi/3}^T$ are the transpose of $T_{2\pi/3}$ and $T_{-2\pi/3}$, respectively. $C_{RRR,o}$ is obtained from Eq. (50).

From Eqs. (51) and (52), compliance matrices of link 2 and 3 can be expressed as,

$$C_{RRR2,o} = T_{2\pi/3} \times C_{RRR,o} \times T_{2\pi/3}^T \tag{55}$$

$$C_{RRR3,o} = T_{-2\pi/3} \times C_{RRR,o} \times T_{-2\pi/3}^T \tag{56}$$

Since springs are arranged parallel to each other, the compliance matrix of the 3-RRR compliant micro-motion stage can be found using the rule for calculating the equivalent compliances for parallel connections of springs,

$$C_{3RRR} = (C_{RRR1}^{-1} + C_{RRR2}^{-1} + C_{RRR3}^{-1})^{-1} \tag{57}$$

where $C_{RRR1} = C_{RRR,o}$.

The output displacements due to applied forces/moments can be expressed as,

$$[\Delta x \quad \Delta y \quad \Delta \gamma]_{3RRR}^T = C_{3RRR} \times F_o \tag{58}$$

4. Case studies and comparison of results with FEA

Table 1 shows the geometries and material properties of a RRR and 3-RRR compliant micro-motion stages. All flexure hinges in these micro-motion stages have the same geometries and material properties. Therefore, all flexure hinges have the same compliances of $[\Delta\alpha_z/M_z]_i$, $[\Delta y/F_y]_i$ and $[\Delta x/F_x]_i$ ($i = 1, 2, 3$), respectively. The t/R ratio of all the flexure hinges is 0.63. Four cases were studied where flexure hinge equations developed by [3,7,6,18] and the FEA determined flexure hinge results obtained in this paper were used to estimate the compliances of flexure hinges. Since the flexure hinge compliance results of Paros & Weisbord (full equations) [7], Lobontiu [6] and Wu & Zhou [18] are the same (see Figs. 2–4), the results of this group will be represented by the results of Lobontiu. Table 2 shows the flexure hinge compliances calculated from the chosen hinge equations in each case.

For $\Delta\alpha_z/M_z$, it can be seen in Fig. 2 that at $t/R = 0.63$, the results of Schotborgh’s equation are the closest to the FEA results, followed by Paros and Weisbord’s simplified equation and Lobontiu’s equation. For $\Delta y/F_y$,

Table 1
Geometries and material properties of the compliant micro-motion stages

Geometries/material properties	Value
Young’s modulus, E (GPa)	71.7
Poisson’s ratio, ν	0.33
l_1 (mm)	15.5
l_2 (mm)	8
l_3 (mm)	10.5
l_4 (mm)	28
l_6 (mm)	27
t_1, t_2, t_3 (mm)	0.94
R_1, R_2, R_3 (mm)	1.5
b (mm)	12.7

Table 2
Flexure hinge compliances calculated using various equations

Case	Chosen flexure hinge equation			Flexure hinge compliance		
	$\Delta\alpha_z/M_z$ (rad/Nm)	$\Delta y/F_y$ (m/N)	$\Delta x/F_x$ (m/N)	$\Delta\alpha_z/M_z$ (rad/Nm)	$\Delta y/F_y$ (m/N)	$\Delta x/F_x$ (m/N)
Case 1	Sch [3]	Sch [3]	Sch [3]	0.0254	1.561×10^{-8}	4.143×10^{-9}
Case 2	PW (simplified) [7]	PW (simplified) [7]	PW (simplified) [7]	0.0222	4.994×10^{-8}	1.534×10^{-9}
Case 3	Lob [6]	Lob [6]	Lob [6]	0.0204	5.155×10^{-8}	2.402×10^{-9}
Case 4	Sch [3]	FEA determined	FEA determined	0.0254	7.190×10^{-8}	2.415×10^{-9}

Sch: Schotborgh et al., PW: Paros and Weisboard and Lob: Lobontiu.

and $\Delta x/F_x$, it can be seen in Figs. 3 and 4 that the results of Lobontiu’s equations are the closest to the FEA results, followed by Paros & Weisbord’s (simplified) and Schotborgh’s equations. The results of Schotborgh’s equations for $\Delta y/F_y$ and $\Delta x/F_x$ have large differences when compared to the FEA and the analytical results of Paros & Weisbord (simplified) and Lobontiu. This is because Schotborgh’s equations consider different aspects of the hinge compared to the others. Nevertheless, the discussion of Schotborgh et al.’s modelling method is beyond the scope of this paper.

The output compliances of the RRR and 3-RRR micro-motion stages are calculated using the flexure hinge equations aforementioned to study the effect of the accuracy of these hinge equations on the output compliances. The results of the analytical output compliances of the stages are shown in Tables 3–5. These analytical compliances are compared to the FEA results.

Table 3
Comparison between analytical and FEA results for the RRR micro-motion stage

Flexure hinge compliance equation	Analytical output compliance matrix (m/N, m/Nm, rad/N, rad/Nm)			% difference		
Case 1: Sch [3]	3.669×10^{-5}	3.117×10^{-5}	-1.603×10^{-3}	-0.6	-0.9	-0.3
	3.117×10^{-5}	3.958×10^{-5}	-1.628×10^{-3}	-0.9	-1.3	-0.9
	-1.603×10^{-3}	-1.628×10^{-3}	7.634×10^{-2}	-0.3	-0.9	-0.3
Case 2: PW (simplified) [7]	3.234×10^{-5}	2.719×10^{-5}	-1.398×10^{-3}	-13.1	-13.6	-13.0
	2.719×10^{-5}	3.449×10^{-5}	-1.421×10^{-3}	-13.6	-14.0	-13.6
	-1.398×10^{-3}	-1.421×10^{-3}	6.659×10^{-2}	-13.0	-13.6	-13.0
Case 3: Lob [6]	2.978×10^{-5}	2.503×10^{-5}	-1.287×10^{-3}	-19.9	-20.5	-19.9
	2.503×10^{-5}	3.174×10^{-5}	-1.308×10^{-3}	-20.5	-20.8	-20.4
	-1.287×10^{-3}	-1.308×10^{-3}	6.130×10^{-2}	-19.9	-20.4	-19.9

Sch: Schotborgh, PW: Paros and Weisboard and Lob: Lobontiu.

Table 4
Comparison between analytical and FEA results for the 3-RRR micro-motion stage

Flexure hinge design equation	Analytical output compliance matrix (m/N, m/Nm, rad/N, rad/Nm)			% difference		
Case 1: Sch [3]	5.676×10^{-7}	0	0	-11.4	-	-
	0	5.676×10^{-7}	0	-	-11.4	-
	0	0	3.593×10^{-4}	-	-	-13.1
Case 2: PW (simplified) [7]	5.091×10^{-7}	0	0	-20.5	-	-
	0	5.091×10^{-7}	0	-	-20.5	-
	0	0	3.226×10^{-4}	-	-	-22.0
Case 3: Lob [6]	4.720×10^{-7}	0	0	-26.3	-	-
	0	4.720×10^{-7}	0	-	-26.3	-
	0	0	2.992×10^{-4}	-	-	-27.6

Sch: Schotborgh et al., PW: Paros and Weisboard and Lob: Lobontiu.

Table 5
Case 4 – Comparison between analytical and FEA results for the two micro-motion stages

Case 4	Analytical output compliance matrix (m/N, m/Nm, rad/N, rad/Nm)			% difference		
RRR	3.711×10^{-5}	3.117×10^{-5}	-1.603×10^{-3}	-0.3	-0.9	-0.3
	3.117×10^{-5}	3.966×10^{-5}	-1.628×10^{-3}	-0.9	-1.1	-0.9
	-1.603×10^{-3}	-1.628×10^{-3}	7.633×10^{-2}	-0.3	-0.9	-0.3
3-RRR	6.193×10^{-7}	0	0	-3.3	-	-
	0	6.193×10^{-7}	0	-	-3.3	-
	0	0	3.953×10^{-4}	-	-	-4.4

4.1. Finite element analysis (ANSYS)

A FEA model was generated using ANSYS. The stage was generated using 8-node, two-dimensional, plane elements (PLANE82) with two DOFs on each node, which are translations in the nodal x - and y -directions. Meshes, constraints and applied forces/moments of the FEA model are shown in Fig. 11. Unit forces/moments are applied at output point o and the corresponding nodal deformations at the point were read. The output compliance matrix of the RRR and 3-RRR micro-motion stages determined using FEA are shown in Eqs. (59) and (60), respectively.

$$C_{RRR_{[FEA]}} = \begin{bmatrix} 3.720 \times 10^{-5} & 3.146 \times 10^{-5} & -1.608 \times 10^{-3} \\ 3.15 \times 10^{-5} & 4.010 \times 10^{-5} & -1.644 \times 10^{-3} \\ -1.608 \times 10^{-3} & -1.644 \times 10^{-3} & 7.653 \times 10^{-2} \end{bmatrix} \tag{59}$$

$$C_{3RRR_{[FEA]}} = \begin{bmatrix} 6.405 \times 10^{-7} & 0 & 0 \\ 0 & 6.405 \times 10^{-7} & 0 \\ 0 & 0 & 4.134 \times 10^{-4} \end{bmatrix} \tag{60}$$

The off-diagonal compliances of $C_{3RRR_{[FEA]}}$ in Eq. (60) are very small and insignificant compared to the diagonal terms. Therefore, the off-diagonal compliances are assumed to be zero. This is expected as the 3-RRR compliant stage has a RCC (remote-centre-of-compliance) configuration and deformations occur only along the direction of the applied force/moment [20].

Analytical output compliances calculated from Eqs. (50) and (57) using the chosen flexure hinge equations (see Table 2) were compared with FEA results. The differences between the analytical and the FEA results are shown in Tables 3–5.

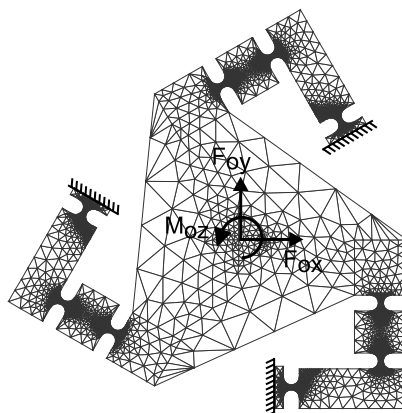


Fig. 11. FEA model of 3-RRR compliant micro-motion stage.

4.1.1. Results and discussions

The results in Tables 3 and 4 show that the analytical output compliances of RRR and 3-RRR compliant stages calculated using Schotborgh et al.'s flexure hinge equations are the closest to the FEA results, followed by Paros & Weisbord's (simplified) and Lobontiu's equations. The accuracies of the output compliance results follow the trend of the accuracies of the hinge equation, $\Delta\alpha_z/M_z$, but not the accuracies of $\Delta y/F_y$ and $\Delta x/F_x$.

The large differences of output compliances (when compared to FEA results) obtained using Paros and Weisbord's simplified equations are expected because the t/R ratio of flexure hinges in this case is large, which violates the assumption of these analytical equations. The output compliances of the stages calculated using Lobontiu's equations produce larger differences compared to that of Schotborgh's equations. However, Lobontiu's equations may produce accurate results if it would be used to calculate compliances of flexure hinges with t/R ratio other than 0.63.

The $\Delta y/F_y$ and $\Delta x/F_x$ equations of Schotborgh et al. have large differences compared to the FEA determined compliances for $t/R = 0.63$ as shown in Figs. 3 and 4. The large differences (approximately 80%) in the $\Delta y/F_y$ and $\Delta x/F_x$ results do not cause large discrepancies in the output compliance results of the micro-motion stages. In order to study the degree of discrepancies of the output compliances due to Schotborgh et al.'s $\Delta y/F_y$ and $\Delta x/F_x$ equations, these two flexure hinge equations in case 1 are replaced by the FEA determined $\Delta y/F_y$ and $\Delta x/F_x$ and this new case is referred to as case 4. The calculated output compliances for case 4 are shown in Table 5.

From Table 5, it can be seen that the output compliance results of case 4 for the RRR stage are similar to that of case 1. This suggests that, for this particular geometry of the RRR stage, the accuracies of the $\Delta y/F_y$ and $\Delta x/F_x$ have insignificant effects on the output compliances of the stage. The axial and transverse deformations of the flexure hinges are very small and insignificant to influence the results of the output compliances of the RRR stage. Meanwhile, the output compliances of case 4 for the 3-RRR stage are closer to the FEA results compared to that of case 1. The maximum difference of the output compliance results in case 4 is 4.4% compared to 13% in case 1. This suggests that for this particular 3-RRR stage, the accuracies of the $\Delta y/F_y$ and $\Delta x/F_x$ have some effects on the output compliances of the stage (but not up to the extend of 80%). The axial and transverse deformations of flexure hinges are small but are significant enough to have small influences to the results of the output compliances of the 3-RRR stage. As a conclusion, accurate output compliances of the 3-RRR micro-motion stage can be obtained when the suitable flexure hinge equations are used.

Results in Tables 3–5 also show the advantage of the closed-form output compliance equations of the micro-motion stages presented in this paper. The flexure hinge equations, $\Delta\alpha_z/M_z$, $\Delta y/F_y$ and $\Delta x/F_x$ are variables in the output compliance equations. Therefore, researchers can choose the most suitable flexure hinge compliance equation by referring to Figs. 2–4 (based on the t/R ratio of the flexure hinges) in order to accurately calculate the output compliances of the micro-motion stages.

5. Conclusions

The effect of the accuracies of flexure hinge equations on the output compliances of micro-motion stages are studied. Simple closed-form equations are derived in this paper to determine the output compliances of a RRR and a 3-RRR micro-motion stage. The flexure hinge equations, $\Delta\alpha_z/M_z$, $\Delta y/F_y$ and $\Delta x/F_x$ are variables in the output compliance equations of the stages; therefore flexure hinge compliance equations with different accuracies (which vary with the t/R ratios of hinges) can be used to calculate the output compliances. It was found that the accuracy of the output compliances mainly influenced by the accuracies of the $\Delta\alpha_z/M_z$ equations. It was also found that the accuracies of the $\Delta y/F_y$ and $\Delta x/F_x$ equations have insignificant effects on the accuracies of the output compliances of the RRR stage. However, the accuracies of these equations influence the accuracies of the output compliances of the 3-RRR stage. As a conclusion, accurate output compliances of the 3-RRR micro-motion stage can be obtained when the most suitable flexure hinge equation are used. The suitable flexure hinge equations can be chosen (based on the t/R ratio of the flexure hinges) by referring to Figs. 2–4.

Experiments will be conducted in the near future to further justify the accuracies of the presented output compliance results. Closed-form equations of calculating the input compliances of the stages are derived. The

effect of the accuracies of flexure hinge equations on the input compliances of micro-motion stages will be presented in near future.

Acknowledgements

The authors greatly acknowledge the support of the Adelaide Robotics Research Group at the University of Adelaide and the use of its facilities. The authors also acknowledge the instrumentation and workshop staff at the School of Mechanical Engineering for all their help. Also, a special thanks to George Osborne for his innovative ideas and excellent craftsmanship.

References

- [1] Y.M. Tseytlin, Notch flexure hinges: an effective theory, *Review of Scientific Instruments* 73 (9) (2002) 3363–3368.
- [2] I. Her, J.C. Chang, A linear scheme for the displacement analysis of micropositioning stages with flexure hinges, *Journal of Mechanical Design Transactions of the ASME* 116 (1994) 770–776.
- [3] W.O. Schotborgh, F.G. Kokkeler, H. Tragter, F.J. van Houten, Dimensionless design graphs for flexure elements and a comparison between three flexure elements, *Precision Engineering* 29 (2005) 41–47.
- [4] S. Smith, D. Chetwynd, D. Bowen, Design and assessment of monolithic high precision translation mechanisms, *Journal of Physics E: Scientific Instruments* 20 (1987) 977–983.
- [5] F.-Z. Hsiao, T.-W. Lin, Analysis of a novel flexure hinge with three degrees of freedom, *Review of Scientific Instruments* 72 (2) (2001) 1565–1573.
- [6] N. Lobontiu, *Compliant Mechanisms: Design of Flexure Hinges*, CRC Press, 2003.
- [7] J.M. Paros, L. Weisbord, How to design flexure hinges, *Machine Design* 37 (1965) 151–156.
- [8] F. Scire, E. Teague, Piezodriven 50- μm range stage with subnanometer resolution, *Review of Scientific Instruments* 49 (12) (1978) 1735–1740.
- [9] E. Furukawa, M. Mizuno, T. Doi, Development of a flexure-hinged translation mechanism driven by two piezoelectric stacks, *JSME International Journal, Series C: Dynamics, Control, Robotics, Design and Manufacturing* 34 (4) (1995) 743–748.
- [10] R. Yang, M. Jouaneh, R. Schweizer, Design and characterisation of a low-profile micropositioning stage, *Precision Engineering* 18 (1996) 20–29.
- [11] W. Zhang, J. Zou, L. Watson, W. Zhao, The constant-jacobian method for kinematics of a three-DOF planar micro-motion stage, *Journal of Robotic Systems* 19 (2) (2002) 63–72.
- [12] H.-H. Pham, I.-M. Chen, H.-C. Yeh, Micro-motion selective-actuation XYZ flexure parallel mechanism: design and modeling, *Journal of Micromechatronics* 3 (1) (2005) 51–73.
- [13] M. Jouaneh, R. Yang, Modeling of flexure-hinge type lever mechanisms, *Precision Engineering* 27 (2003) 407–418.
- [14] N. Lobontiu, E. Garcia, Analytical model of displacement amplification and stiffness optimization for a class of flexure-based compliant mechanisms, *Computers and Structures* 81 (2003) 2797–2810.
- [15] P. Gao, S. Swei, Z. Yuan, A new piezodriven precision micropositioning stage utilizing flexure hinges, *Nanotechnology* 10 (1999) 394–398.
- [16] H.-H. Pham, I.-M. Chen, Stiffness modeling of flexure parallel mechanism, *Precision Engineering* 29 (2005) 467–478.
- [17] J.W. Ryu, D. Gweon, K.S. Moon, Optimal design of a flexure hinge based $xy\theta$ wafer stage, *Precision Engineering* 21 (1997) 18–28.
- [18] Y. Wu, Z. Zhou, Design calculations for flexure hinges, *Review of Scientific Instruments* 73 (8) (2002) 3101–3106.
- [19] S.T. Smith, V.G. Badami, J.S. Dale, Y. Xu, Elliptical flexure hinges, *Review of Scientific Instruments* 68 (3) (1997) 1474–1483.
- [20] W.-K. Kim, B.-J. Yi, W. Cho, RCC characteristics of planar/spherical three degree-of-freedom parallel mechanisms with joint compliances, *Journal of Mechanical Design* 122 (2000) 10–16.